[5]Launder, B. E., and Sharma, B. I., "Application of the Energy-Dissipation Model of Turbulence to the Calculation of Flow near a Spinning Disk," *Letters in Heat and Mass Transfer*, Vol. 1, 1974, pp. 131–138.

[6]Nagano, Y., and Kim, C., "A Two-Equation Model for Heat Transport in Wall Turbulent Shear Flows," *Journal of Heat Transfer*, Vol. 110, No. 3, 1988, pp. 583–589.

[7]Yap, C. R., "Turbulent Heat and Momentum Transfer in Recirculating and Impinging Flows," Ph.D. Dissertation, Faculty of Technology, Univ. of Manchester, Manchester, England, UK, 1987.

[8]Piccin, O., and Cassoudensalle, D., "Etude Dans La Soufflerie F1 Des Profiles AS329 et A240," ONERA, PV 73/1685A YG, Toulouse, France, 1987.

[9]Cook, P. H., McDonald, M. A., and Firmin, M. C. P., "Airfoil RAE2822—Pressure Distributions, and Boundary Layer and Wake Measurements," AGARD-AR 138, 1979.

Computational Simulation of the F-22 Aircraft

Eswar Josyula* and Raymond E. Gordnier†
U.S. Air Force Research Laboratory,
Wright–Patterson Air Force Base, Ohio 45433-7913

Introduction

ACCURATE computational fluid dynamic (CFD) studies of a full aircraft must take into account a good strategy for solving the fluid dynamic equations, ease of grid generation, appropriate turbulence model, and computer capabilities to resolve the flowfield. Subsonic flows at high angle of attack are dominated by effects of vortical structures and possible vortex breakdown. Vortex breakdown severely effects the aircraft stability and control and may reduce the operational envelope of high-performance flight. This problem is particularly relevant to twin-tailed fighters where the tails could be immersed in unsteady flow resulting from the bursting of vortices generated upstream, known as tail buffet.

In this Note, a computational simulation has been performed for the complete aircraft configuration of the F-22. The external flowfield about the aircraft at subsonic speeds and high angle of attack (up to 30-deg incidence) is studied. The effect of yaw on the vortex trajectories is also investigated. Important flowfield details such as the location and strength of the vortical structures are studied qualitatively to elucidate the flow physics and demonstrate the capability of the CFD technology. Results are compared with experimental data[1] for validation of the flow solver. More extensive details about the information presented in this note can be found in the Ref. 2.

The governing equations are taken to be the unsteady three-dimensional, compressible, mass-averaged Navier–Stokes equations. A two-equation k-ε turbulence[3] model is used for the present study. The two-equation model is used because an explicit length-scale specification required for an algebraic model can be difficult to determine and ambiguous for complex geometries involving multiple grids. The mass-averaged Navier–Stokes equations are solved using the numerical code, FDL3DI, which is based on the implicit Beam and Warming algorithm[4] and employs a domain decomposition strategy to handle complex geometries.

Results and Discussion

The flow conditions for the numerical simulation are given in Table 1. The Reynolds number was based on the reference length c of the wing root chord of the model. The full-scale length of the root chord is 240 in. All conditions were selected based on the availability of experimental data.[1] The experiment consisted of a wind-tunnel test of a 0.10-scale model without stores. For the purpose of validation, the surface pressure coefficient measured by the experiment was used.

The grids were generated from a CAD source of the original geometry using the GRIDGEN software.[5] The computation departed from the original geometry only with respect to the engine inlet and outlet. In the computation, a freestream inflow condition was specified at the inlet face with the outflow capped. Overlapping grids were constructed for the various components of the F-22 aircraft, viz. nose, fuselage, inlet, wing, and horizontal and vertical tails. All grids except the nose and inlet grids were of H topology, the nose was C-O topology, and the inlet grids were rectangular. The entire mesh system was embedded within a background mesh extending five root chord lengths away from the body in all directions, except the spanwise direction, which extended two root chord lengths. A minimum distance, $\Delta y/c = 4.6 \times 10^{-5}$, was used in the body normal direction, resulting in $y^+ = 10$ at the first y-mesh point above the surface. Here, c, is the reference length of the wing root chord referred to earlier. Solution convergence was assumed for the high-alpha turbulent solutions when the vortex on the downstream of the aircraft did not change between two solutions three characteristic times apart. All turbulent solutions were started from converged laminar solutions. The data processing rate is 2.6×10^{-5} CPU-seconds/step/node for the turbulent computation on a single processor of the Cray T-90 computer.

The comparison of surface pressure on the upper surface for the experiment[1] and computation is shown in Fig. 1 for an angle of attack of 20 deg. Results at 10- and 30-deg angle of attack are found in Ref. 2. Because of calculations having bilateral symmetry, it is possible to show top views of the F-22 aircraft with one side of the symmetry plane showing the experiment and the other side the computation.

The comparison shows good qualitative agreement between the experiment and computation, and trends given by the experiment are captured in the CFD predictions. Comparison of the computational and experimental surface pressures on the forebody are good. Both experiment and computation display a low-pressure footprint

Table 1 Flow conditions and grid details

Mach number	Re_∞	α, deg	β, deg	Number of nodes, $\times 10^6$	Blocks
0.4	4.6×10^6	10	0	1.0	6
0.4	4.6×10^6	20	0	1.0	6
0.4	4.6×10^6	30	0	1.0	6
0.6	4.6×10^6	24	0	2.0	12
0.6	4.6×10^6	24	6	2.0	12

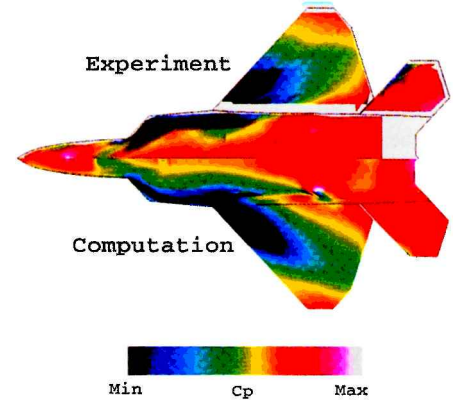

Fig. 1 Top view of comparison of surface pressure. $M_\infty = 0.4$ and $\alpha = 20$ deg.

Presented as Paper 98-0526 at the AIAA 36th Aerospace Sciences Meeting, Reno, NV, Jan. 12–15, 1998; received Aug. 3, 1998; revision received Dec. 11, 1998; accepted for publication Dec. 15, 1998. This paper is declared a work of the U.S. Government and is not subject to copyright protection in the United States.

*Research Aerospace Engineer, AFRL/VAAC, 2645 Fifth Street, Suite 7. E-mail: josyule@vaa.wpafb.af.mil.

†Research Aerospace Engineer, AFRL/VAAC, 2645 Fifth Street, Suite 7.

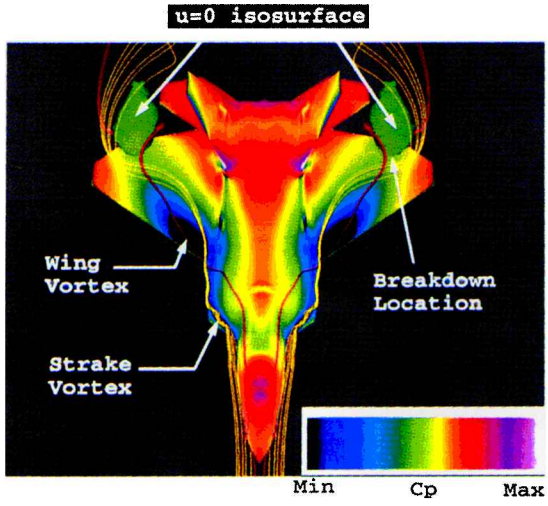

Fig. 2 Top view of particle traces, surface pressure, and three-dimensional representation of vortex breakdown. Mach number = 0.4 and α = 20 deg.

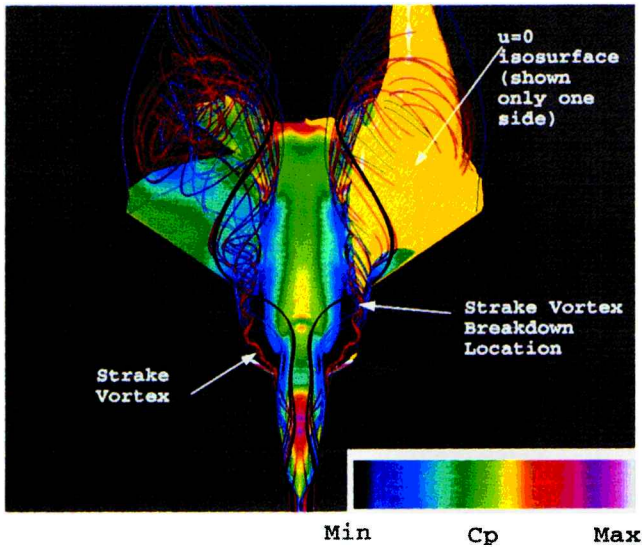

Fig. 3 Top view of particle traces, surface pressure, and three-dimensional representation of vortex breakdown. Mach number = 0.4 and α = 30 deg.

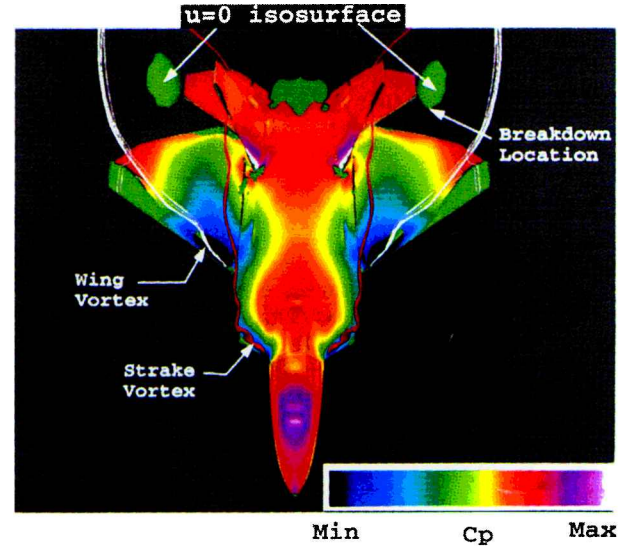

Fig. 4 Top view of particle traces, surface pressure, and three-dimensional representation of vortex breakdown. Mach number = 0.6, α = 24 deg, and β = 0 deg.

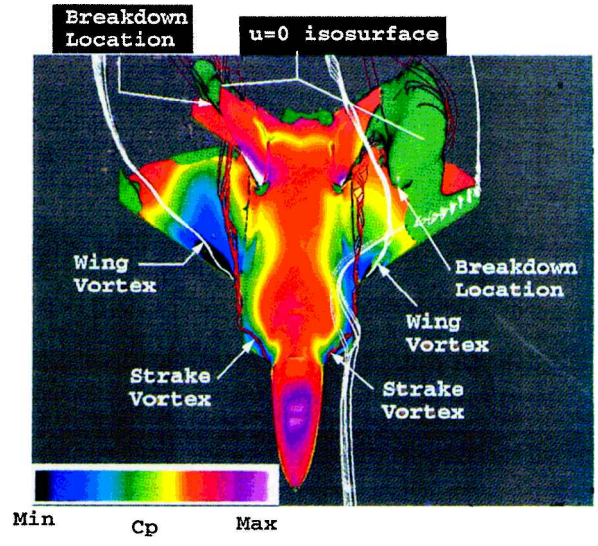

Fig. 5 Top view of particle traces, surface pressure, and three-dimensional representation of vortex breakdown. Mach number = 0.6, α = 24 deg, and β = 6 deg.

on the strake. This feature indicates the development and strengthening of the leading-edge vortical structures with increasing angle of attack. The comparison of the magnitude and extent of the computed and experimental low-pressure region on the strake is good. The low-pressure footprint at the leading edge of the wing observed in experiment is predicted well. The trajectory of the computed vortex indicated by the low-pressure region on the wing (Fig. 1), matches that of the experiment. The overall comparison of the results at 10, 20, and 30 deg shows the development of significant low-pressure regions on the surface with increasing angle of attack.

To study the effect of angle of attack, a freestream Mach number of 0.4 and angles of attack of 10, 20, and 30 deg were computed. At the lower angle of attack of 10 deg, only relatively weak vortices were generated by the strake. Figures 2 and 3 show the predicted surface pressure contours and streamlines for the 20- and 30-deg cases, respectively. Particles were released in the core of the vortices to study the trajectories of the different vortices. The tightly spiraling streamlines along the low-pressure region on the nose (30-deg case), strake, and wing (20- and 30-deg case, respectively) show the path of the vortical structures. Also indicated in the figures are regions of reversed u velocity highlighted by the green and yellow isosurfaces of $u = 0$.

For the 20-deg case shown in Fig. 2, the strake vortex runs along the strake leading edge and onto the wing. Over the wing, the strake vortex merges with the wing vortex. The merging of these vortices over the wing is distinguished by the coalescence of the two distinct, low total pressure zones (not shown here). Toward the rear of the wing these merged vortices undergo vortex breakdown. This leads to the development of the negative u-velocity region seen in Fig. 2.

For the 30-deg case shown in Fig. 3, a small vortex develops along the forebody, resulting in a low-pressure region along the side of the canopy. In the computation, this vortex dissipates farther downstream. A stronger strake vortex is formed as indicated by the lower-pressure region on the strake. This vortex breaks down slightly upstream of the wing leading edge, as seen from the extent of upstream penetration of the reversed u-velocity zone (Fig. 3). The flow over the wing is also almost fully stalled and has a reduced influence on the strake vortex. Therefore, the broken-down strake vortex tracks more inboard and the vertical tail is immersed in this flow.

For a freestream Mach number of 0.6- and 24-deg angle of attack, sideslip angles β of 0 and 6 deg (port side forward computed) are considered to study the effect of yaw. At $\alpha = 24$ deg and $\beta = 0$, a strake vortex is formed (Fig. 4). The vortex path traverses the wing

and is located outboard of the vertical tail. For a sideslip angle $\beta = 6$ deg (Fig. 5), a stronger vortex is formed on the port side strake. The trajectory of this vortex is located more inboard on the wing/fuselage and passes just outboard of the port side vertical tail. This results in a region of lower pressure on the outboard side toward the root of the vertical tail (figure not shown). Furthermore, over the wing, a more extensive stalled flow region (Fig. 5) exists for the $\beta = 6$-deg case, leading to higher pressures on the port side wing than for $\beta = 0$ case. This is due to the effectively lower sweep of the port side wing for $\beta = 6$ deg.

On the starboard side, the effect of yaw is to move the trajectory of the strake vortex farther outboard of the vertical tail. The wing vortex also moves slightly farther outboard and is weaker, resulting in no vortex breakdown. This is due to a higher sweep angle for the starboard wing at $\beta = 6$ deg. The stalled flow region at the tip of the wing is also less extensive for the $\beta = 6$-deg case.

References

[1] Bryant, M. D., Arendt, L. L., and Hobbs, R. W., "Wing Tunnel Test of a 0.10-Scale F-22 Aircraft Pressure Model (L3) With and Without Stores," Arnold Engineering Development Center, AEDC-TSR-93-P3, Arnold AFB, TN, Jan. 1993.

[2] Josyula, E., and Gordnier, R. E., "Computational Simulation of the F-22 Aircraft," AIAA Paper 98-0526, Jan. 1998.

[3] Jones, W. P., and Launder, B. E., "The Prediction of Laminarization with a Two-Equation Model of Turbulence," *International Journal of Heat and Mass Transfer*, Vol. 15, No. 2, 1972, pp. 301–314.

[4] Beam, R. M., and Warming, R. F., "An Implicit Factored Scheme for the Compressible Navier-Stokes Equations," *AIAA Journal*, Vol. 16, No. 4, 1978, pp. 393–402.

[5] Steinbrenner, J. P., Chawner, J. P., and Fouts, C. L., "The GRIDGEN 3D Multiple Block Grid Generation System, Volume II: User's Manual," Wright Research and Development Center, TR-90-3022, Flight Dynamics Lab., Wright–Patterson AFB, OH, Feb. 1991.

Color reproductions courtesy of Wright–Patterson Air Force Base.